

Spatial Frequency-Dependent Signal-to-Noise Ratio as a Generalized Measure of Image Quality

Philipp Bernhardt*, Lothar Bätz, Ernst-Peter Rührnschopf**, Martin Hoheisel
Siemens AG Medical Solutions, Erlangen/Forchheim, Germany

ABSTRACT

A generalized, objective image quality measure can be defined for X-ray based medical projection imaging: the spatial frequency-dependent signal-to-noise ratio $SNR = SNR(u,v)$. This function includes the three main image quality parameters, i.e. spatial resolution, object contrast, and noise. The quantity is intimately related to the DQE concept, however its focus is not to characterize the detector, but rather the detectability of a certain object embedded into a defined background. So also effects from focus size and radiation scatter can be quantified by this method. The $SNR(u,v)$ is independent of basic linear post-processing steps such as appropriate windowing or spatial filtering. The consideration of the human visual system is beyond the scope of this concept.

By means of this quantity, different X-ray systems and setups can be compared with each other and with theoretical calculations. Moreover, X-ray systems (i.e. detector, beam quality, geometry, anti-scatter grid, basic linear post-processing steps etc.) can be optimized to deliver the best object detectability for a given patient dose.

In this paper $SNR(u,v)$ is defined using analytical formulas. Furthermore, we demonstrate how it can be applied with a test phantom to a typical flat panel detector system by a combination of analytical calculations and Monte Carlo simulations.

Finally the way this function can be used to optimize an X-ray imaging device is demonstrated.

Keywords: Medical X-ray imaging, image quality measure, DQE , contrast, noise, spatial resolution

1. INTRODUCTION

For the optimization of the setup of a medical projection X-ray imaging device it is always a challenge to find a good compromise between image sharpness and noise level¹. For example a large focal spot size guarantees a high quantum flux and, hence, a reduced noise level. On the other hand, image resolution suffers from a poorly conditioned source. A second example addresses motion blurring: A fast moving object appears blurred, if the exposure time is very long, on the other hand a short pulse leads to inappropriately high noise levels. In this paper an objective image quality measure is introduced, which is derived from the DQE concept²: The spatial frequency-dependent signal-to-noise ratio $SNR = SNR(u,v)$. This function includes the three main image quality parameters: spatial resolution, object contrast, and noise, and allows these three quantities to be balanced.

2. DEFINITION: $SNR(u,v)$

The objective quality of medical X-ray images is basically determined by three parameters: spatial resolution, contrast, and noise. These three parameters can be integrated in a single function, the frequency dependent signal to noise ratio $SNR = SNR(u,v)$. This function describes the ratio between the signal and the noise detected in the X-ray image dependent on the two dimensional spatial frequencies u and v .

* philipp.bernhardt@siemens.com; phone: +49-9191-18-9746; fax: +49-9191-18-8951

** Consultant to Siemens AG Medical Solutions

Let $H(u,v)$ be the Fourier transform of the deterministic signal $h(x,y)$ and $NPS(u,v)$ the corresponding noise power spectrum, $SNR(u,v)$ can be calculated by:

$$(1) \quad SNR(u,v) = \frac{|H(u,v)|}{\sqrt{NPS(u,v)}}$$

The noise power spectrum is, in fact, only defined if the underlying signal is spatially invariant. The object of interest, however, absorbs more or less radiation than the background. Hence, the noise power spectrum is different at that location. Assuming that the object of interest is small and the signal difference to the background is also small, the noise power spectrum can be determined at the position of a sufficiently large, homogeneous background area.

$SNR(u,v)$ obviously includes spatial resolution and noise. The contrast, in terms of the signal difference, is incorporated in the spatial frequency dependent signal. A high contrast results in strong signal amplitude in the corresponding frequency band. The linearity between contrast (signal difference) and $SNR(u,v)$ is a consequence of the following mathematical relation:

$$(2) \quad \begin{aligned} \text{signal} &\Leftrightarrow \text{modulus of the Fourier transform} \\ h(x,y) &\Leftrightarrow |H(u,v)| \\ a \cdot h(x,y) + b &\Leftrightarrow |a \cdot H(u,v) + b \cdot \delta(u) \cdot \delta(v)|. \end{aligned}$$

For u or v unequal to zero, the modulus of $H(u,v)$ is proportional to any signal scaling.

$SNR(u,v)$ is invariant to linear deterministic image-processing algorithms. Neither a variation of image brightness or contrast, nor the application of spectral filters (high pass filter, low pass filter, harmonization, etc.) have any influence on the frequency-dependent $SNR(u,v)$.

The relationship to the term “detective quantum efficiency $DQE(u,v)$ ” is obvious. The $DQE(u,v)$ describes the performance properties of a detector, whereas $SNR(u,v)$ is focused on the complete X-ray imaging system and setup, measuring its ability to detect a certain object. Expressed mathematically: $SNR(u,v)$ is the signal to noise ratio at the detector exit, whereas $DQE(u,v)$ is the ratio between the squared $SNR(u,v)$ values at the exit and at the entrance of the detector:

$$(3) \quad DQE(u,v) = \frac{SNR_{out}^2(u,v)}{SNR_{in}^2(u,v)}$$

$SNR(u,v)$ is, like $DQE(u,v)$, not a single number, but a function. In this paper the spatial frequencies u and v of the function $SNR(u,v)$ refer to the detector plane.

To be able to use this parameter as a real score card for an X-ray system and setup, it must be decided, which spatial resolution, i.e. which spatial frequency region is most important for the actual detection problem. If thin guide wires have to be observed, the function $SNR(u,v)$ should be analyzed also for higher spatial frequencies. Imaging of soft tissue, on the other hand, requires large $SNR(u,v)$ values in the low frequency domain. Furthermore it is important to know whether the object itself or details of an object have to be imaged, e.g. a possible stenosis in the vascular system.

3. DERIVATION OF $SNR(u,v)$ FOR INDIRECT-DETECTION FLAT PANEL DETECTORS

3.1. Important parameters

The following list gives an overview of the most important parameters for $SNR(u,v)$, using a pulsed-source X-ray imaging system:

- object (guide wires, stents, contrast-media-filled vessels with iodine or CO_2 , etc.)
- source-to-image distance (SID)
- geometrical magnification factor of the object
- size of the detector
- patient thickness
- tube voltage U
- pre-filter, material and thickness
- tube current I
- exposure time t

The first five variables are more or less defined by the attending physicist (“task parameters”), the last four variables can either be selected manually or chosen by an automatic exposure control of the X-ray imaging device (“optimization parameters”).

3.2. Geometrical model

For the calculation of $SNR(u,v)$ the following geometrical model is used: The background is represented by a cube, consisting of pure water, Lucite, or a mixture of soft tissue and bones, i.e. materials, whose absorption properties are close to those of the human body. The thickness of the cube defines the patient thickness. An appropriate simplified shape for the objects of interest such as guide wires or vessels is a cylinder, whose axis is rectangular to the beam direction. It is situated in the center of the cube. The complete layout is illustrated in [Figure 1](#).

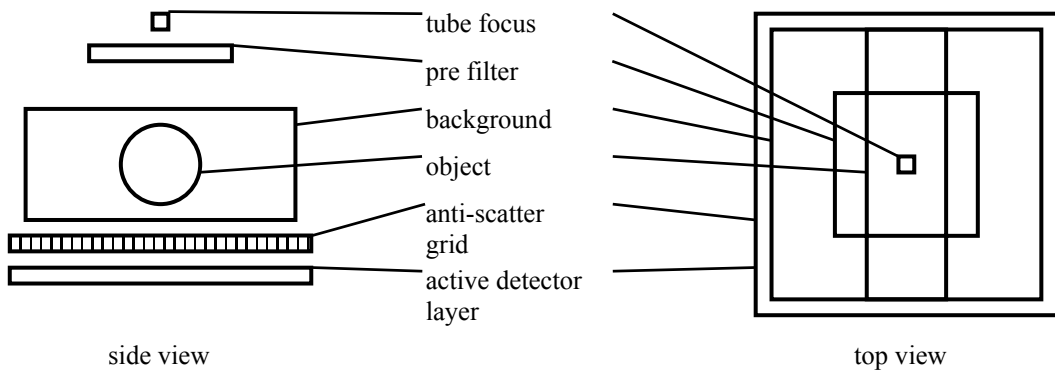


[Figure 1](#): Sketch of the geometrical model

3.3. Calculation procedure

Because of the limited calculation power of present-day computers, it is not possible to simulate a complete X-ray image by a pure Monte Carlo track-structure calculation technique for the determination of $SNR(u,v)$. Hence, the problem is solved by a combination of three different strategies:

- deterministic calculations
- stochastic (=Monte Carlo track structure) simulations
- analytical calculations (cascaded model)

The whole process of the calculation of $SNR(u,v)$ is illustrated in [Figure 2](#).

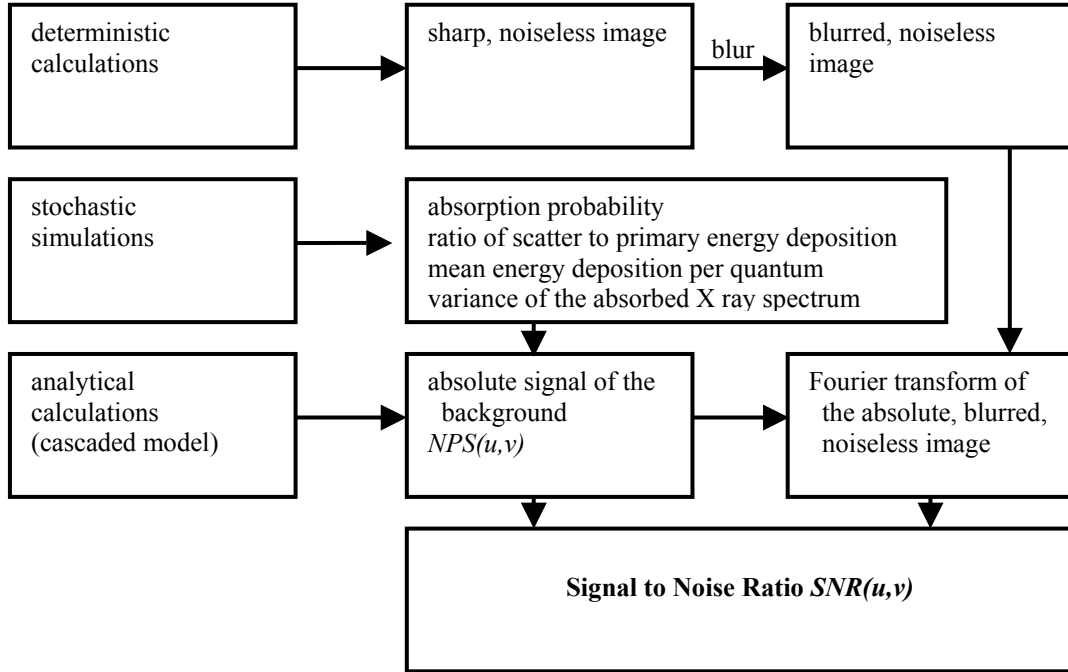


Figure 2: Sketch of the calculation procedure of $SNR(u, v)$

3.3.1. Deterministic calculations

A pencil-shaped X-ray beam from the focal spot to the center of the detector pixel is considered for every detector pixel. With the help of material composition, density, and thickness in the beam, it is possible to calculate the average probability of primary X-ray quanta with an energy spectrum defined by the tube setup (anode material, anode angle, tube voltage) being registered in the active layer of the detector. The absolute signal height can not be determined by the deterministic calculations, since scatter radiation is missing. To avoid sampling effects due to a finite pixel size at that stage, the real pixel length is reduced. To summarize, the result of this deterministic calculation is an extremely sharp, noiseless X-ray image, given in relative intensities. The Siemens-internal program “DRASIM”^{2,3} is used for the deterministic calculations. The primary X-ray spectra can be taken from Boone et al.⁴ or Aichinger et al.⁵.

Subsequently the perfect images are analytically blurred. The blurring is done in the frequency domain. Therefore the images are Fourier transformed and scaled with the corresponding $MTF(u, v)$ functions, whereby (u, v) are the spatial frequencies in x and y direction, respectively. For the determination of the MTF function, the following Fourier transform of a rectangular input function with base length a is helpful:

$$(4) \quad FT \left\{ rect \left(\frac{x}{a} \right) \right\} = FT \left\{ \begin{cases} 1, & x < \frac{a}{2} \\ 0, & x \geq \frac{a}{2} \end{cases} \right\} = a \cdot \sin c(a f) = a \cdot \frac{\sin(\pi a f)}{\pi a f}$$

Four blurring sources are considered: the focal spot, motion blurring, scattering of quanta in the detector, and detector pre-sampling.

Let f_x and f_y be the sizes of a rectangular focal spot and γ the magnification factor of the object of interest ($\gamma=1 \Rightarrow$ object is directly on the surface of the detector; $\gamma=2 \Rightarrow$ object is exactly half way between focal spot and the detector) such that the corresponding MTF is:

$$(5) \quad MTF_{foc}(u, v) = \sin c(f_x(\gamma - 1)u) \cdot \sin c(f_y(\gamma - 1)v)$$

Let m_x and m_y be the velocity of the object of interest rectangular to the X-ray beam direction, t the exposure time, and γ the above defined magnification factor such that the corresponding MTF is:

$$(6) \quad MTF_{mot}(u, v) = \sin c(m_x t \gamma u) \cdot \sin c(m_y t \gamma v)$$

X-ray quanta and optical quanta in the case of an indirect-detection detector cause blurring. A real corresponding $MTF_{sci}(u, v)$ is difficult to calculate due to the lack of a precise description of the optical properties of the scintillator⁶. Instead of doing so, it should be measured. If energy dependent scattering of X-ray quanta in the active layer and variable interaction depths in the scintillator are neglected a single MTF function for all quanta with different energies and absorption depths can be defined.

Let a_x and a_y be the sizes of the active regions of a detector pixel such that the corresponding MTF is:

$$(7) \quad MTF_{pix}(u, v) = \sin c(a_x u) \cdot \sin c(a_y v)$$

3.3.2. Stochastic simulations

The stochastic simulations are based on Monte Carlo track structure calculations. Here the direction and the energy of the emitted X-ray quanta are randomly chosen from given angle and energy distributions. Then the complete history of this primary and all possible secondary particles is tracked, i.e. all photon interactions (photoelectric effect, coherent scattering, incoherent scattering, K fluorescence) with the pre-filter, the background object, the anti-scatter grid and finally the active layer of the detector are simulated to determine the energy deposition distribution. The object of interest can be omitted in these simulations, since its total influence is assumed to be negligibly small. The statistics, obtained by tracking approximately 10^8 quantum histories are good enough to find out the following system properties, assuming the scatter radiation is homogeneously distributed over the whole detector area:

- number of absorbed quanta N (primary and secondary quanta) in the active layer of the detector per emitted primary quantum
- ratio S/P between secondary energy deposition and primary energy deposition in the active layer of the detector
- mean deposited energy $\langle E \rangle$ per absorbed quantum
- variance of energy σ_E^2 of absorbed quanta

The Siemens internal program "MOCASSIM"^{2,3} is used for the stochastic simulations.

3.3.3. Analytical calculation (cascaded model)

The influence of the physical processes in the flat-panel detector on the uniform image (without an object of interest) can be described with the help of a linear cascaded model^{7,8}. The process is divided into five steps, i.e. the conversion of the X-ray quanta to optical quanta in the scintillator, scattering of optical quanta in the scintillator, selection of light quanta, spatial integration of interacting light quanta, and output of the discrete detector elements.

In every step both the quantum flux q (mean number of particles per unit area) and the corresponding noise power spectrum $NPS(u,v)$ are updated. The input parameters q_0 and $NPS_0(u,v)$ can be calculated with the help of the number of absorbed quanta N , the SID , the X-ray tube gain Q for a certain tube voltage (1/mAs/sr), the tube current I , and the exposure time t :

$$(8) \quad q_0 = \frac{N \cdot Q \cdot I \cdot t}{(SID)^2}$$

$$NPS_0(u,v) = \frac{N \cdot Q \cdot I \cdot t}{(SID)^2}$$

The conversion of the X-ray quanta into optical quanta can be split into two gain processes: Firstly, the energy of the quantum is distributed via secondary particles (mainly electrons). Secondly, optical transitions, caused by the electrons in the scintillator, generate optical quanta⁹.

The gain factor for the energy deposition is equivalent to the mean deposited energy $\langle E \rangle$ per primary X-ray quantum, the variance σ_E^2 of this process is dependent on the width of the absorbed spectrum. Both values are determined during the statistical simulations.

The mean gain factor $\langle G \rangle$ for the generation of optical quanta is dependent on the scintillator material; it is given in optical quanta per absorbed energy. In the case of CsI, $\langle G \rangle$ is approximately 55/keV¹⁰. Under the assumption of Poisson statistics the variance of this distribution is $\sigma_G^2 = \langle G \rangle$.

It is important to note, that both these gain processes always have to be combined. The energy deposition is, in fact, not a real gain process, since energy units and not particles are produced. It is only justified by immediate application of a second gain process. The resulting quantum flux q_1 and NPS_1 are

$$(9) \quad q_1 = \langle E \rangle \langle G \rangle q_0$$

$$NPS_1(u,v) = \langle E \rangle^2 \langle G \rangle^2 NPS_0(u,v) + \langle G \rangle^2 \sigma_E^2 q_0 + \sigma_G^2 \langle E \rangle q_0$$

Assuming a unique $MTF_{sci}(u,v)$ for all optical quanta inside the scintillator, the resulting quantum flux q_2 and NPS_2 are:

$$(10) \quad q_2 = q_1$$

$$NPS_2(u,v) = (NPS_1(u,v) - q_1) \cdot MTF_{sci}^2(u,v) + q_1$$

The probability β for the detection of the optical quanta includes the coupling efficiency of light from the scintillator as well as the quantum efficiency of the detector array. This gain process results in the following flux q_3 and NPS_3 :

$$(11) \quad q_3 = \beta q_2$$

$$NPS_3(u,v) = \beta^2 (NPS_2(u,v) - q_2) + \beta q_2$$

The detector pre-sampling signal corresponds to the spatial integral over the active region of a detector pixel with width of a_x and a_y , respectively. The new flux q_4 and the NPS_4 equals

$$(12) \quad q_4 = a_x a_y q_3$$

$$NPS_4(u,v) = a_x^2 a_y^2 NPS_3(u,v) \cdot \sin c^2(a_x u) \cdot \sin c^2(a_y v)$$

Finally, the discrete detector signal is recorded. Let p_x and p_y , respectively, be the distances between the center of two neighboring pixels such that the expected digital signal value q_5 of a pixel and the digital NPS_5 are:

$$(13) \quad q_5 = q_4$$

$$NPS_5(u, v) = NPS_4(u, v) + \sum_{n_x=1}^{\infty} \sum_{n_y=1}^{\infty} NPS_4 \left(u \pm \frac{n_x}{p_x}, v \pm \frac{n_y}{p_y} \right)$$

3.3.4. Final calculation of $SNR(u, v)$

With the help of scatter-to-primary ratio S/P and q_5 , intensities of the noiseless, blurred image can be scaled. Assuming that the object of interest is small and the scatter radiation is homogeneously distributed over the whole image area, a constant amount of scatter, which is the product of the actual background intensity and S/P , is added to all pixels of the image. Then the image is scaled to achieve a background intensity of q_5 , whereby the artificially reduced pixel length of the deterministic calculation (see 3.3.1.) has to be considered. The Fourier transform $H(u, v)$ can now be determined from the resulting scaled image. Finally, $SNR(u, v)$ can be calculated:

$$(14) \quad SNR(u, v) = \frac{|H(u, v)|}{\sqrt{NPS_5(u, v)}}$$

For every point in the exposure parameter space (see chapter 3.1.) the function $SNR(u, v)$ can thus be obtained. The results can be used to find the optimum parameter setup for the X-ray imaging device.

Electronic noise, which is independent of detector dose, was neglected in this derivation, which is justified only for sufficiently high detector dose. Nevertheless, the model could be easily extended to include these effects.

4. EXAMPLE: MOTION BLURRING VERSUS HIGH-DOSE IMAGING

The advantage of the image quality parameter $SNR(u, v)$ defined here is the ability to find the best compromise between image sharpness and noise. In the following example the optimal exposure time is determined for the detection of moving guide wires, typically used in cardiology. Let the guide wires have a cylindrical shape, a diameter of d , and a velocity m rectangular to their axes; the magnification factor of the system is γ . The tube voltage and the tube current are fixed in this example.

Since a constant motion can be fully described in one dimension, it is sufficient to determine the influence of the exposure time t on the one-dimensional function $SNR(u)$, whereby u is the correspondent spatial frequency with respect to the direction of motion. The exposure time t affects $SNR(u)$ in two ways:

- A long exposure time generates blurring, because the object is moving (see 3.3.1.). For a constant tube current during the X-ray pulse the influence on $SNR(u)$ can be described by:

$$(15) \quad SNR(u) \propto \sin c(mu \gamma t)$$

- Increasing the exposure time raises contrast and noise level (see Equation 8). In total, according to Equation 14, $SNR(u)$ behaves like:

$$(16) \quad SNR(u) \propto t \cdot \frac{1}{\sqrt{t}} = \sqrt{t}$$

Equation 15 and 16 can now be combined:

$$(17) \quad SNR(u) \propto \frac{\sin(\pi mu \gamma t)}{\pi mu \gamma \sqrt{t}}$$

Now one can think of the optimal exposure time. Therefore, the dependence of $SNR(u)$ on exposure time t is given in [Figure 3](#) for a fixed spatial frequency u , a velocity m of the object, and a magnification factor γ .

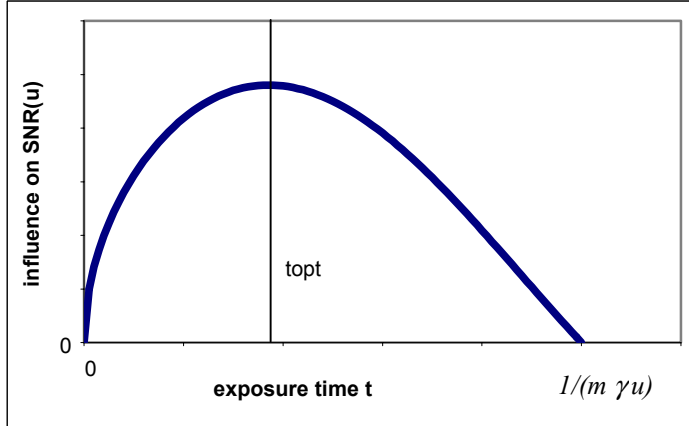


[Figure 3](#): Influence of the exposure time t on $SNR(u)$ for a given spatial frequency u , a velocity m of the object, and a magnification factor γ .

With increasing exposure time the number of quanta rises. Therefore the object dominates more and more over the background noise. Further increase of the exposure time leads to enhanced motion blurring, deteriorating the image quality. Hence, there is an optimal value t_{opt} for the exposure time, which is given by:

$$(18) \quad t_{opt} \approx \frac{0.37}{m \gamma u}$$

Equation 18 is a result of an analysis of a transcendental equation, which leads to the coefficient of 0.37.

Now this result for t_{opt} shall be illustrated. Therefore, a spatial frequency or the center of a frequency band have to be found, which is, e.g. important for the detection of a guide wire. The frequency, whose half wave length is equal to the size γd of the guide wire in the detector plane is presumably a major contributor. Hence, $u = \frac{1}{2d\gamma}$, and Equation 18 can be rewritten as:

$$(19) \quad t_{opt} \approx \frac{0.74 d}{m}$$

d/m is the time period, which is necessary for one edge of the guide wire to pass the original position of the other edge. Hence the most adequate exposure time for imaging moving guide wires is given, when there is an overlap of approximately 25% between the guide wire at the beginning and at the end of the exposure, independently of the magnification factor. [Figure 4](#) illustrates this statement. Assuming a typical diameter d of 0.36 mm and a typical average velocity m of 40 mm/s (see [Figure 5](#)) in cardiology the optimum exposure time is approximately 6.7 ms, which is in good agreement with published measurements¹¹.

Finally in [Figure 6](#) the example is simulated with the help of the DRASIM^{2,3} program. The exposure time is varied from 0.5 ms to 18 ms. The object in this simulation is a set of parallel orientated guide wires in front of a homogeneous background, moving perpendicular to their axis. Whereas detectability increases up to 6.3 ms, motion blurring effects dominate beyond. Finally, at 18 ms individual guide wires are no more visible.

The idea of using a set of guide wires instead of a single guide wire was prompted by the fact, that this periodical object is mainly based on the spatial frequency around $u = \frac{1}{2d\gamma}$, whereas a single guide wire also includes low-frequency

components. These components would profit from long exposure times. Consequently, the detectability of a single guide wire in front of a homogeneous background could even rise with increasing exposure time, even though the guide wire becomes more and more blurred. A real anatomical image, however, includes anatomical noise and structures, typically with high amplitude at lower spatial frequencies, as shown in [Figure 7](#). Therefore, it is recommended to focus the optimization on the intrinsic spatial frequencies for a guide wire around $u = \frac{1}{2d\gamma}$.

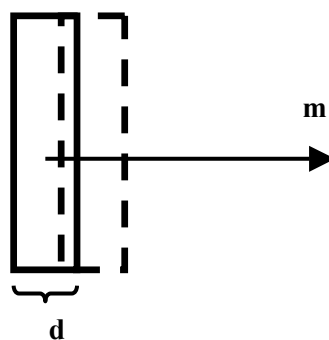


[Figure 4](#): Illustration of the optimal exposure time of a guide wire moving perpendicular to its axis. The solid line represents the position of the guide wire at the beginning of the exposure, the broken line gives the position at the end of the exposure.

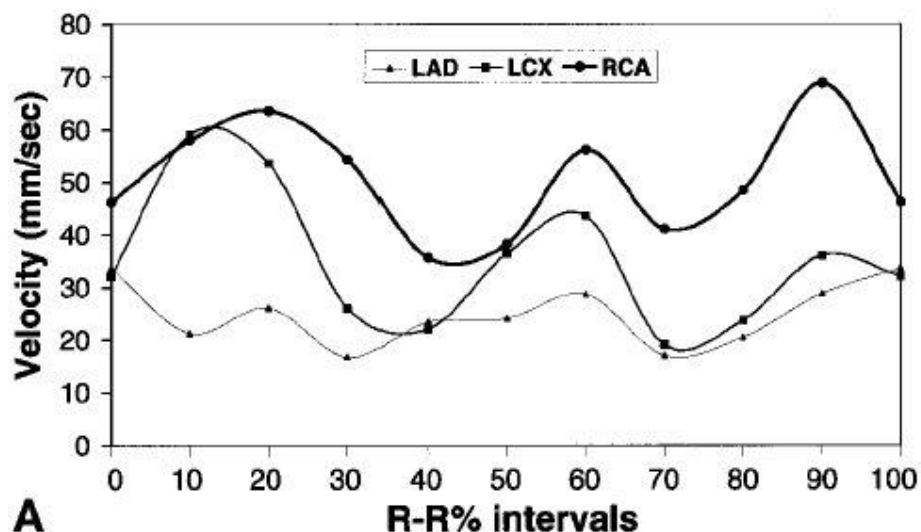
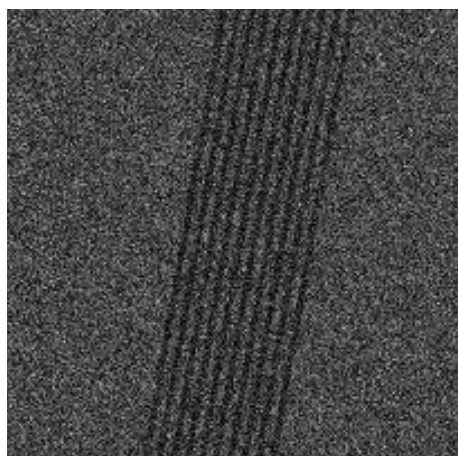
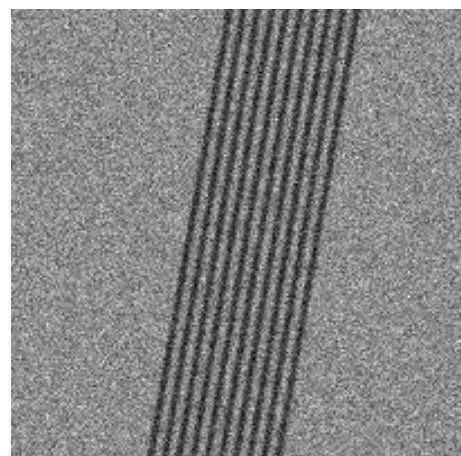


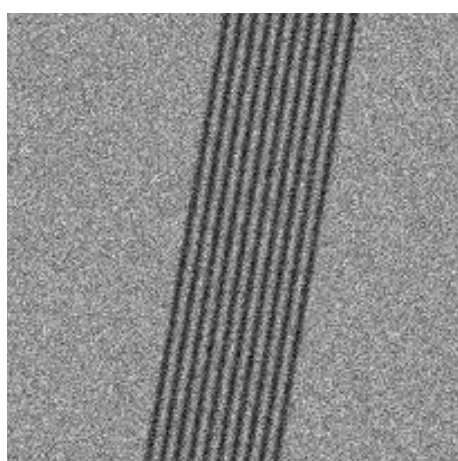
[Figure 5](#): Copy of Fig.2 of Lu et al.¹²: Velocity of a cardiac cycle for different regions of the heart at 72 beats per minute. (LAD=left anterior descending coronary artery; LCX=left circumflex; RCA=right coronary artery)



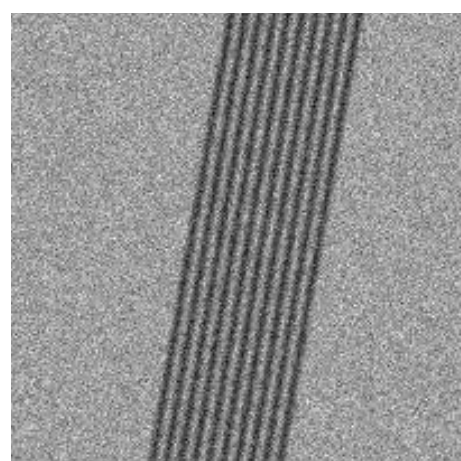
0.5 ms



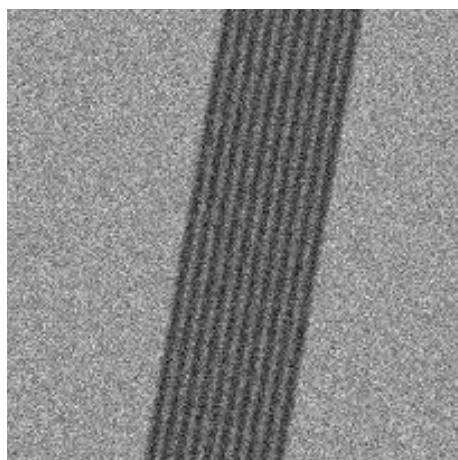
4.5 ms



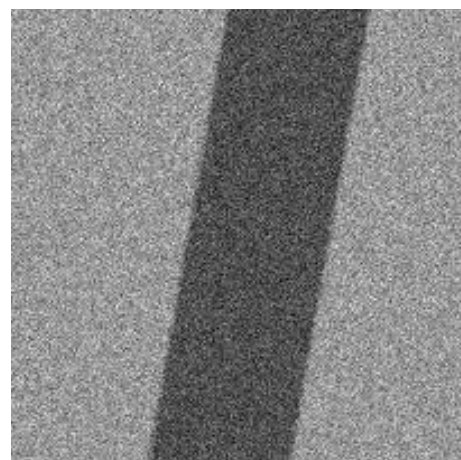
6.3 ms



9.0 ms



13.5 ms



18.0 ms

Figure 6: Images of moving guide wires ($d=0.36$ mm, $m=40$ mm/s) with different exposure times t .

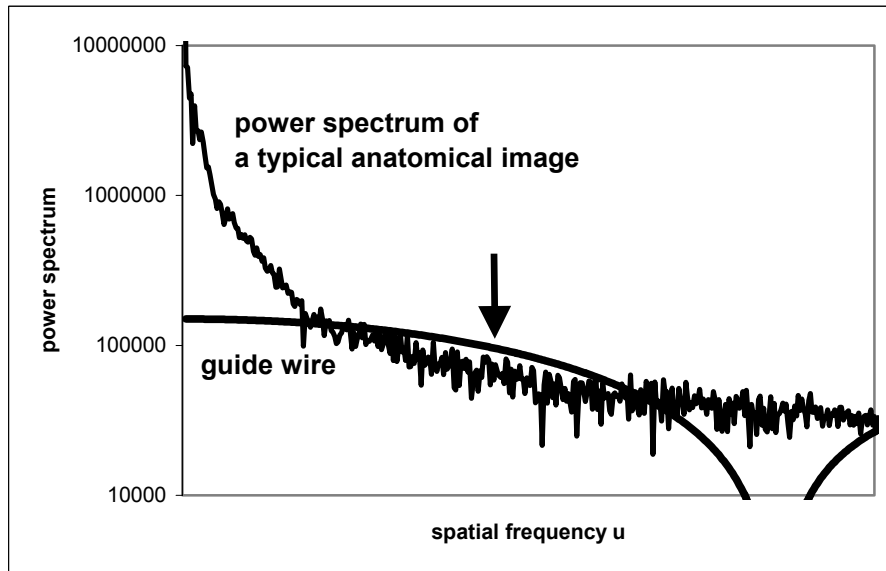


Figure 7: Power spectra of a typical anatomical image and a single guide wire. The arrow indicates the spatial frequency $u=1/(2 d \gamma)$.

5. CONCLUSIONS

In this paper a generalized, objective image quality measure for X-ray based medical projection imaging is introduced: The spatial frequency-dependent signal-to-noise ratio $SNR = SNR(u, v)$. This function has its origins in the *DQE* concept. It combines the three main objective image quality parameters: spatial resolution, object contrast, and noise. Besides the analytical definition, it was demonstrated, how this function can be calculated for a test phantom at a typical flat-panel detector system by applying a combination of analytical calculations and Monte Carlo simulations. At the end an example is given, in which way the function $SNR(u, v)$ can be used to optimize a pulsed X-ray imaging device. For a moving object, the most suitable exposure time was determined.

ACKNOWLEDGEMENTS

The authors would like to thank Thomas Mertelmeier and Wolfgang Härrer (both Siemens AG) for stimulating discussions and valuable comments. We are indebted to Mary Murphy for reviewing the manuscript.

REFERENCES

1. C.L. Gordon, "Image quality optimization using an x-ray spectra model based optimization method", Proc. of SPIE **3977**, 456-465, 2000
2. K. Stierstorfer, T. Flohr, H. Bruder, "Segmented multiple plane reconstruction: A novel approximate reconstruction scheme for multi-slice spiral CT", Phys Med Biol **7**, 2571-2581, 2002
3. T. Flohr, B. Ohnesorge, H. Bruder, K. Stierstorfer, J. Simon, C. Suess, S. Schaller, "Image reconstruction and performance evaluation for ECG-gated spiral scanning with a 16-slice CT system", Med Phys **30**, 2650-2662, 2003
4. J.M. Boone, J.A. Seibert, "An accurate method for computer-generating tungsten anode x-ray spectra from 30 to 140 kV", Med Phys **24**, 1661-1670, 1997
5. H. Aichinger, J. Dierker, S. Joite-Barfuss, M. Säbel, *Radiation Exposure and Image Quality in X-Ray Diagnostic Radiology*, Springer Verlag, Berlin 2004

-
- 6. R.K. Swank, "Calculation of Modulation Transfer Functions of X-Ray Fluorescent Screens", *Applied Optics* **12**, 1865-1870, 1973
 - 7. I.A. Cunningham, "Applied Linear-Systems Theory", *Handbook of Medical Imaging*, J. Beutel, H.L. Kundel, R.L. Van Metter, Volume 1, 79-160, SPIE Press, Washington 2000
 - 8. I.A. Cunningham, J. Yao, V. Subotic, "Cascaded Models and the DQE of Flat-Panel Imagers: Noise Aliasing, Secondary Quantum Noise and Reabsorption", Proc. of SPIE **4682**, 61-70, 2002
 - 9. M. Hoheisel, J. Giersch, P. Bernhardt, "Intrinsic spatial resolution of semiconductor X-ray detectors: a simulation study", *Nuclear Instruments and Methods in Physics Research A* **531/1-2**, 75-81, 2004
 - 10. J.A. Rowlands, "Flat Panel Detectors for Digital Radiography", *Handbook of Medical Imaging*, J. Beutel, H.L. Kundel, R.L. Van Metter, Volume 1, 223-328, SPIE Press, Washington 2000
 - 11. E. Guibelalde, E. Vano, F. Vaquero, L. Gonzalez, "Influence of x-ray pulse parameters on the image quality for moving objects in digital cardiac imaging", *Med Phys* **31**, 2819-2825, 2004
 - 12. B. Lu, S.S. Mao, N. Zhuang, H. Bakhsheshi, H. Yamamoto, J. Takasu, S.C. Liu, M.J. Budoff, "Coronary artery motion during the cardiac cycle and optimal ECG triggering for coronary artery imaging", *Invest Radiol* **36**, 250-256, 2001